AIP Advances

Impact of Cattaneo-Christov heat flux in the flow over a stretching sheet with variable thickness

T. Hayat, M. Farooq, A. Alsaedi, and Falleh Al-Solamy

Citation: AIP Advances **5**, 087159 (2015); doi: 10.1063/1.4929523
View online: http://dx.doi.org/10.1063/1.4929523
View Table of Contents: http://scitation.aip.org/content/aip/journal/adva/5/8?ver=pdfcov
Published by the AIP Publishing

Impact of Cattaneo-Christov heat flux in the flow over a stretching sheet with variable thickness

T. Hayat,[1,2] M. Farooq,[1,a] A. Alsaedi,[2] and Falleh Al-Solamy[2]
[1]*Department of Mathematics, Quaid-I-Azam University 45320, Islamabad 44000, Pakistan*
[2]*Nonlinear Analysis and Applied Mathematics (NAAM) Research Group, Department of Mathematics, Faculty of Science, King Abdulaziz University, P. O. Box 80257, Jeddah 21589, Saudi Arabia*

(Received 7 June 2015; accepted 7 August 2015; published online 20 August 2015)

The present analysis concentrates on the boundary layer flow of Maxwell fluid over a stretching sheet with variable thickness. Cattaneo-Christov heat flux model is used instead of classical Fourier's law to explore the heat transfer characteristics with variable thermal conductivity. Suitable transformations are employed to achieve the nonlinear ordinary differential equations. Convergent series solutions of the momentum and energy equations are obtained. Behavior of various pertinent parameters on the velocity and temperature distributions are analyzed and discussed. [http://dx.doi.org/10.1063/1.4929523]

INTRODUCTION

Transfer of heat is an important phenomenon in the nature which exists due to temperature difference between two bodies or within the same body. Characteristics of heat transfer have been explored by Fourier's law[1] of heat conduction in the last two centuries. However this model is not adequate in the sense that any initial disturbance is felt instantly throughout the whole substance. To overcome this difficulty Cattaneo[2] added a thermal relaxation time in the classical Fourier's of heat conduction which allows the transport of heat via propagation of thermal waves with finite speed. After that Christov[3] modified the Cattaneo law by thermal relaxation time along with Oldroyd's upper-convected derivatives in order to achieve the material-invariant formulation. Straughan[4] studied Cattaneo-Christov model with thermal convection. Tibulle and Zampoli[5] provided the uniqueness of Cattaneo-Christov heat flux model for flow of incompressible fluids. Han et al.[6] presented boundary layer stretched flow of Maxwell fluid with Cattaneo-Christov heat flux model. Mustafa[7] explored the characteristics of Cattaneo-Christov heat flux in the rotating flow of Maxwell fluid over a linear stretching sheet.

The analysis of boundary layer stretched flow accompanied with heat transfer has gained the interest of researchers and scientists due to their widespread applications in many areas of manufacturing, industrial, metallurgical and engineering phenomena. Moving surface into a cooling medium is a mathematical tool for the process of heat treatment. During this process metals are heated and cooled in a specific order so that to keep the metal away from molten state. The objective of heat treating process is to make a metal stronger, harder and resistant. Heat treating process is also used to make a metal softer and more ductile. Few applications here comprise of polymer extrusion, glass blowing, crystal growth, paper production, drawing plastic films, annealing and tinning of copper wires, manufacturing artificial fibers, boundary layer along a liquid film in condensation processes and aerodynamic extrusion of plastic sheets etc. In many manufacturing processes, the raw material passes through the die for the extrusion in liquefied state under high temperature. Unsteady boundary layer flow over a permeable stretching sheet with non-uniform

[a]Corresponding author. Tel.: +92 51 90642172. email address: hfarooq99@yahoo.com

heat source/sink is investigated by Zheng et al.[8] Rashidi et al.[9] examined the thermal magnetohydrodynamic (MHD) flow of nanofluid induced by stretching sheet. Su et al.[10] analyzed magnetohydrodynamic mixed convection flow past a permeable stretching wedge with Ohmic heating and thermal radiation. Turkyilmazoglu[11] investigated three-dimensional magnetohydrodynamic flow of viscoelastic fluid over a stretching sheet with different aspects. Magnetohydrodynamic flow past a shrinking surface with velocity slip and temperature jump is studied by Zheng et al.[12] Hayat et al.[13] studied the boundary layer stagnation point flow of Jeffrey fluid over a stretching sheet with convective boundary condition. Zheng et al.[14] examined unsteady radiative mixed convection flow of Maxwell fluid over a permeable stretching plate with slip and non-uniform heat/source effects. Mukhopadhyay et al.[15] explored the solutal stratification effect in the boundary layer flow of viscous fluid over a permeable stretching sheet. Hayat et al.[16] analyzed the stagnation point flow of an Oldroyd-B fluid ina thermally stratified medium. Sheikholeslami and Ganji[17] explored the characteristics of nanofluid in a rotating system with stretching sheet. Although most of the researchers investigated the boundary layer flow over stretching sheets in different configurations but such flow over a stretched sheet with variable thickness is not investigated properly. Variable thickness of the sheet is useful in the mechanical, civil, marine and aeronautical structures and designs. The use of variable thickness helps to reduce the weight of structural elements and improve the utilization of the material. Fang et al.[18] studied the boundary layer flow of viscous fluid induced by stretching sheet with variable thickness. Analysis of slip velocity in the boundary layer flow over a nonlinearly stretching sheet with variable thickness is presented by Khader and Megahed.[19] Characteristics of heat transfer in the flow of nanofluid over a nonlinear stretching sheet with variable thickness are explored by Wahed et al.[20]

The main objective of present analysis is to describe the rheological characteristics of upper-convected Maxwell fluid and Cattaneo-Christov heat flux model in flow over a stretching sheet with variable thickness. Thermal conductivity of the material is assumed variable. Non-similar analytic solutions are obtained by applying homotopic technique.[21–26] Impacts of various pertinent parameters are the velocity and temperature distributions are computed and discussed.

MATHEMATICAL FORMULATION

Consider the incompressible boundary layer flow of Maxwell fluid over a stretching sheet with variable thickness. Unlike the Fourier law of heat conduction Cattaneo-Christov heat flux model is employed to analyze the characteristics of heat transfer. Thermal conductivity of the fluid is assumed variable. Cartesian coordinates are chosen in such a way that x-axis is along the sheet while y-axis is normal to it (see Fig. 1). The conservation laws of mass, linear momentum and

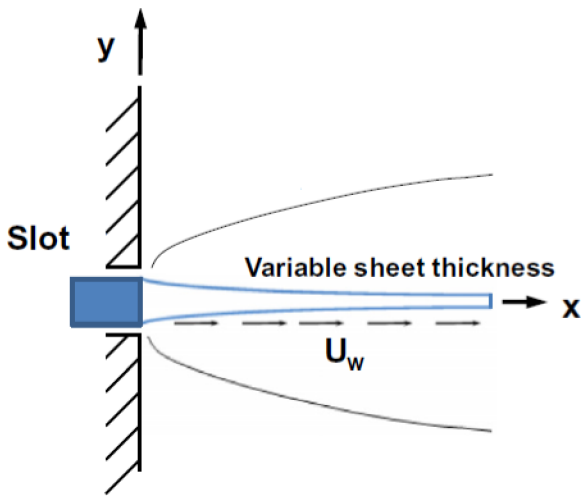

FIG. 1. Physical flow model.

energy are expressed as follows:[6]

$$\frac{\partial u}{\partial x}+\frac{\partial v}{\partial y}=0, \tag{1}$$

$$u\frac{\partial u}{\partial x}+v\frac{\partial u}{\partial y}=\nu\frac{\partial^2 u}{\partial y^2}-\lambda_1\left(u^2\frac{\partial^2 u}{\partial x^2}+v^2\frac{\partial^2 u}{\partial y^2}+2uv\frac{\partial^2 u}{\partial x\partial y}\right), \tag{2}$$

$$\rho c_p \mathbf{v}.\nabla T=-\nabla.\mathbf{q}. \tag{3}$$

The new flux model is known as "Cattaneo-Christov heat flux model" and it has the following form:[3]

$$\mathbf{q}+\lambda_2\left(\frac{\partial \mathbf{q}}{\partial t}+\mathbf{v}.\nabla\mathbf{q}-\mathbf{q}.\nabla\mathbf{v}+(\nabla.\mathbf{v})\ \mathbf{q}\right)=-k\,(T)\,\nabla T, \tag{4}$$

Where λ_2 is the relaxation time of heat flux, $k\,(T)$ is the variable thermal conductivity which depends linearly on temperature. It is noted that for $\lambda_2=0$ Eq. (4) reduces to classical Fourier's law. As it is assumed that fluid is incompressible therefore Eq. (4) takes the form

$$\mathbf{q}+\lambda_2\left(\frac{\partial \mathbf{q}}{\partial t}+\mathbf{v}.\nabla\mathbf{q}-\mathbf{q}.\nabla\mathbf{v}\right)=-k\,(T)\,\nabla T, \tag{5}$$

Comparing Eqs. (3) and (5) and then eliminating q, we get the energy conservation law corresponding to Cattaneo-Christov heat flux model as follows:

$$u\frac{\partial T}{\partial x}+v\frac{\partial T}{\partial y}+\lambda_2\left(u\frac{\partial u}{\partial x}\frac{\partial T}{\partial x}+v\frac{\partial v}{\partial y}\frac{\partial T}{\partial x}+u\frac{\partial v}{\partial x}\frac{\partial T}{\partial y}+v\frac{\partial u}{\partial y}\frac{\partial T}{\partial x}+2uv\frac{\partial^2 T}{\partial x\partial y}+u^2\frac{\partial^2 T}{\partial x^2}+v^2\frac{\partial^2 T}{\partial y^2}\right)$$
$$=\frac{1}{\rho c_p}\frac{\partial}{\partial y}\left(k\,(T)\ \frac{\partial T}{\partial y}\right), \tag{6}$$

The subjected boundary conditions are:[16]

$$u=u_w\,(x)=U_0(x+b)^n,\quad v=0,\quad T=T_w\quad \text{at}\quad y=A(x+b)^{\frac{1-n}{2}},$$
$$u\to 0,\quad T\to T_\infty\quad \text{as}\quad y\to\infty. \tag{7}$$

In the above expressions u and v denote the velocity components in the $x-$ and $y-$ directions respectively, λ_1 is the relaxation time, u_w is the stretching velocity, ν is the kinematic viscosity, b is dimensional constant, n is the velocity power index, ρ is the density, c_p is the specific heat, T is the fluid temperature and T_∞ is the ambient fluid temperature. Where $k\,(T)$ is the variable thermal conductivity which is defined as follows:

$$k\,(T)=k_\infty\,(1+\varepsilon\theta)\,, \tag{8}$$

where k_∞ is the thermal conductivity of the ambient fluid, θ is the dimensionless temperature and ε is a small scalar parameter which shows the influence of temperature on variable thermal conductivity.

Considering the following transformations[16]

$$\psi=\sqrt{\frac{2}{n+1}\nu U_0(x+b)^{n+1}}F\,(\eta)\,,\quad \eta=\sqrt{\frac{n+1}{2}\frac{U_0}{\nu}(x+b)^{n-1}}y,\quad u=U_0(x+b)^n F'\,(\eta)\,,$$
$$v=-\sqrt{\frac{n+1}{2}\nu U_0(x+b)^{n-1}}\left[F\,(\eta)+\eta\frac{n-1}{n+1}F'\,(\eta)\right],\quad \Theta\,(\eta)=\frac{T-T_w}{T_w-T_\infty}, \tag{9}$$

incompressibility condition is satisfied automatically and Eqs. (2), (6), and (7) are reduced to

$$F'''+FF''-\frac{2n}{1+n}F'^2+\beta\left((3n-1)\ FF'F''-\frac{2n\,(n-1)}{n+1}F'^3+\eta\frac{n-1}{2}F'^2F''-\frac{n+1}{2}F^2F'''\right)=0, \tag{10}$$

$$(1+\varepsilon\Theta)\ \Theta''+\varepsilon\Theta'^2+\mathrm{Pr}\,F\Theta'+\mathrm{Pr}\,\gamma\left(\frac{n-3}{2}FF'\Theta'-\frac{n+1}{2}F^2\Theta''\right)=0, \tag{11}$$

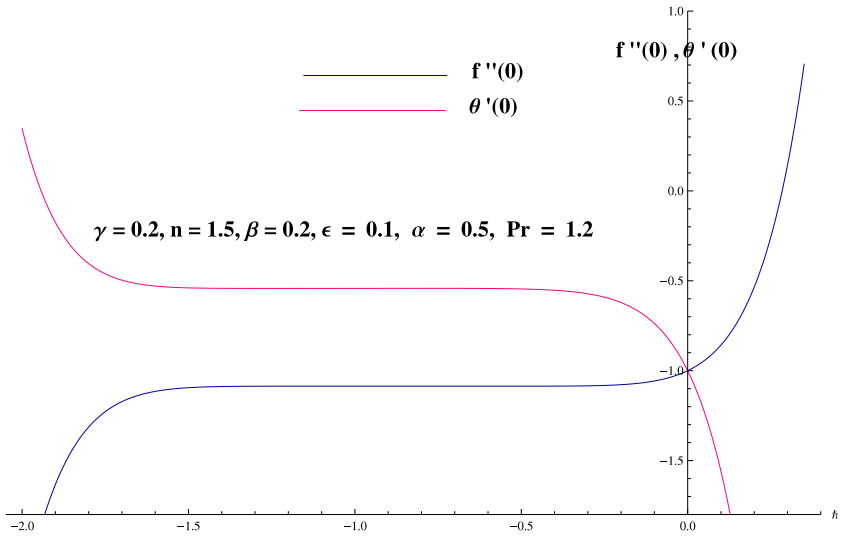

FIG. 2. $\hbar$-curves for f and θ.

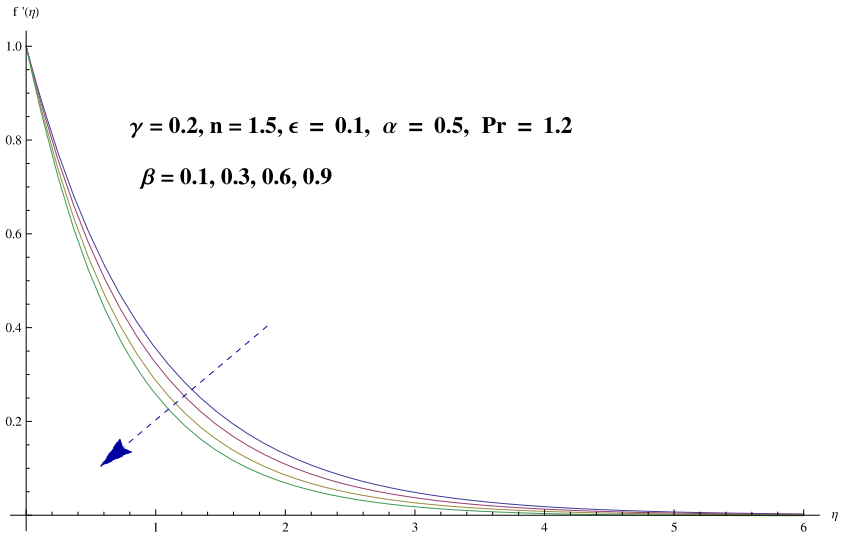

FIG. 3. Effect of β on f'.

$$F(\alpha) = \alpha\frac{(1-n)}{(1+n)}, \quad F'(\alpha) = 1, \quad \Theta(\alpha) = 1,$$
$$F'(\infty) \to 0, \quad \Theta(\infty) \to 0, \tag{12}$$

Where $\alpha = A\sqrt{\frac{n+1}{2}\frac{U_0}{\nu}}$ denotes the plate surface. We define $F(\eta) = f(\eta - \alpha) = f(\xi)$ which reduces the nondimensionlized governing equations and associated boundary conditions as follows:

$$f''' + ff'' - \frac{2n}{1+n}f'^2 + \beta\left((3n-1)\, ff'f'' - \frac{2n(n-1)}{n+1}f'^3 + \eta\frac{n-1}{2}f'^2f'' - \frac{n+1}{2}f^2f'''\right) = 0, \tag{13}$$

$$(1+\varepsilon\theta)\,\theta'' + \varepsilon\theta'^2 + \Pr f\theta' + \Pr\gamma\left(\frac{n-3}{2}ff'\theta' - \frac{n+1}{2}f^2\theta''\right) = 0, \tag{14}$$

$$f(0) = \alpha\frac{(1-n)}{(1+n)}, \quad f'(0) = 1, \quad \theta(0) = 1,$$

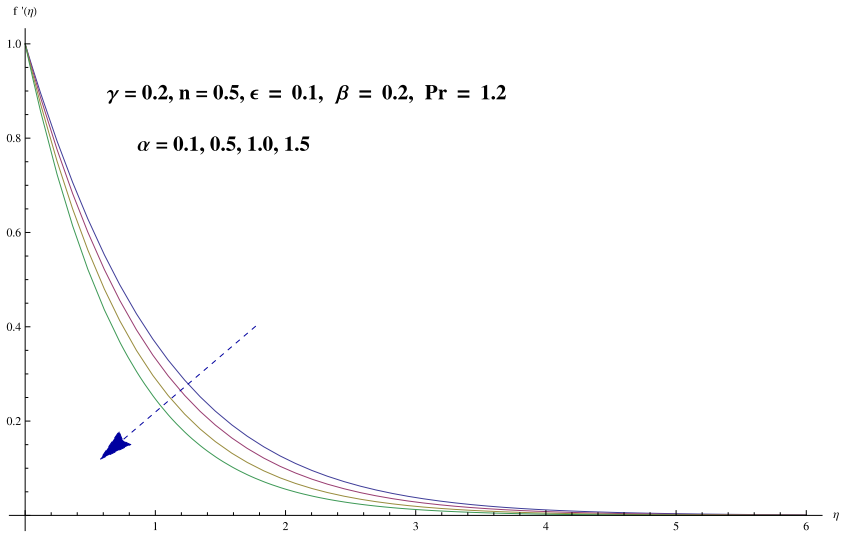

FIG. 4. Effect of α on f'.

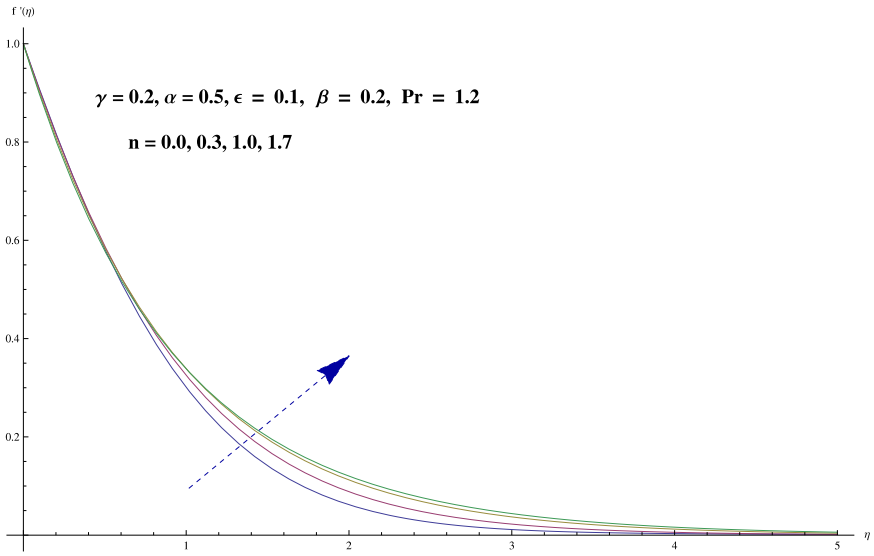

FIG. 5. Effect of n on f'.

$$f'(\infty) \to 0, \quad \theta(\infty) \to 0, \tag{15}$$

where β is the Deborah number in terms of relaxation time, Pr is the Prandtl number and γ is the thermal relaxation parameter. These quantities are expressed as follows:

$$\mathrm{Pr} = \frac{\mu c_p}{k}, \quad \beta = \lambda_1 U_0 (x+b)^{n-1}, \quad \gamma = \lambda_2 U_0 (x+b)^{n-1}. \tag{16}$$

It is noted that for n = 1, the problem reduces to flat plate with same thickness. Also it is noted that for n = 1 and $\varepsilon = 0$, the problem reduces as discussed by Han et al.[6]

HOMOTOPIC SOLUTIONS

Homotopy analysis method was first proposed by Liao[17] in 1992 which is used for the construction of series solution of highly nonlinear problems. To proceed with such method, it is essential to define the initial guesses (f_0, θ_0) and linear operators (L_f, L_θ) for the momentum and energy

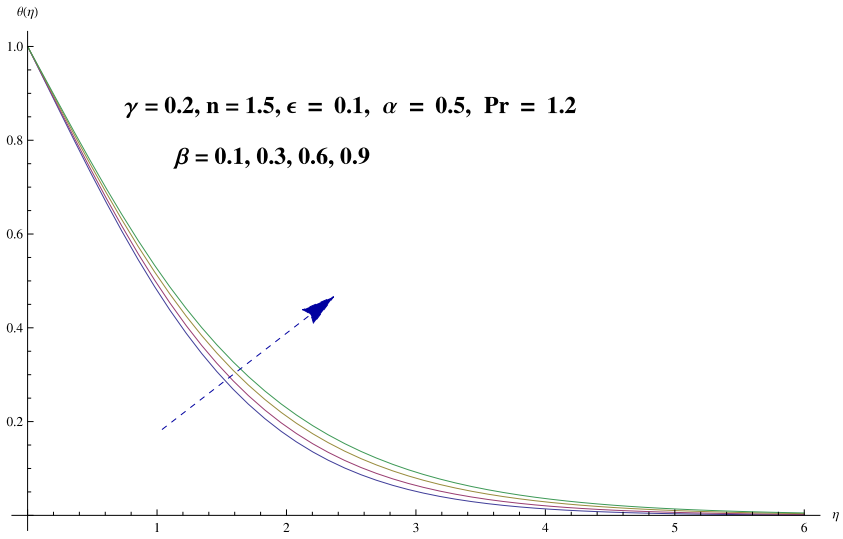

FIG. 6. Effect of β on θ.

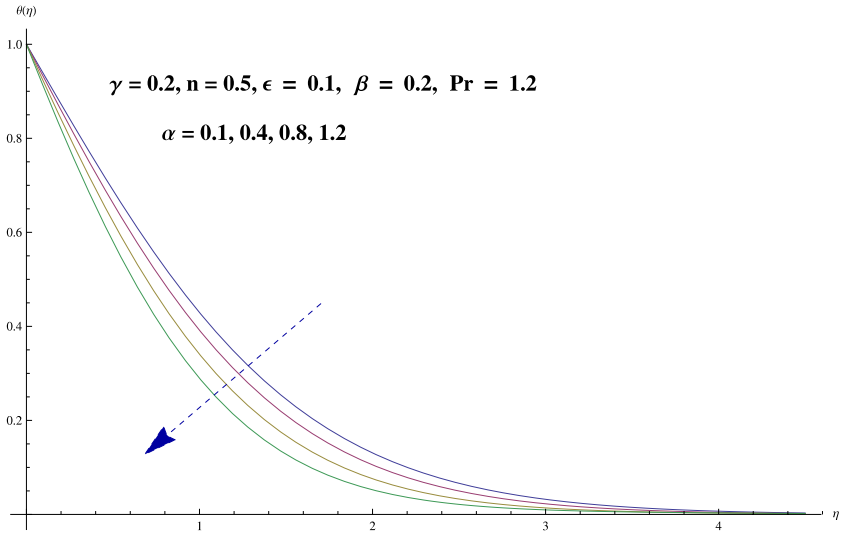

FIG. 7. Effect of α on θ.

equations which are expressed in the forms

$$f_0(\eta) = \alpha\frac{1-n}{1+n} + 1 - \exp(-\eta), \quad \theta_0(\eta) = \exp(-\eta), \tag{17}$$

$$\mathbf{L}_f(f) = \frac{d^3 f}{d\eta^3} - \frac{df}{d\eta}, \qquad \mathbf{L}_\theta(\theta) = \frac{d^2\theta}{d\eta^2} - \theta, \tag{18}$$

with

$$\mathbf{L}_f[A_1 + A_2\exp(\eta) + A_3\exp(-\eta)] = 0, \tag{19}$$

$$\mathbf{L}_\theta[A_4\exp(\eta) + A_5\exp(-\eta)] = 0, \tag{20}$$

where $A_i (i = 1, 2, \ldots, 5)$ are the arbitrary constants. The zeroth and mth order deformation problems are:

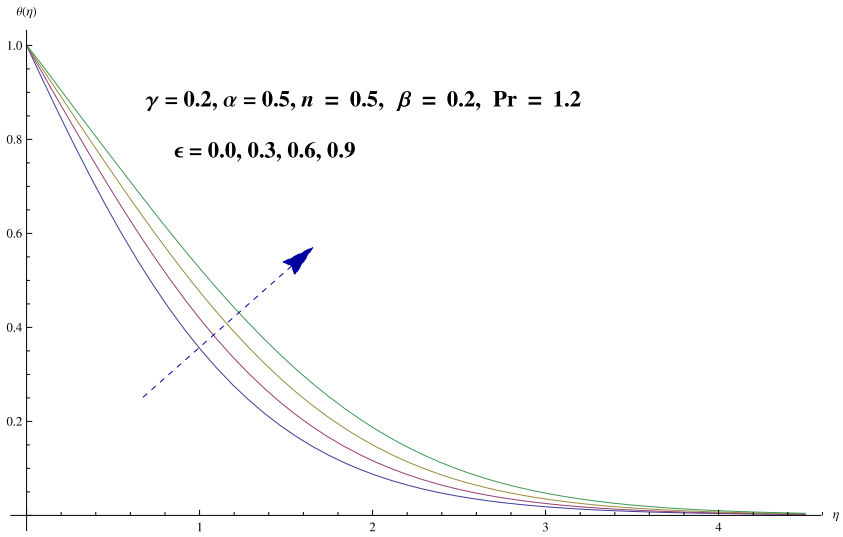

FIG. 8. Effect of ε on θ.

ZEROTH-ORDER PROBLEM

$$(1-p)\mathbf{L}_f[\hat{f}(\eta,p)-f_0(\eta)] = p\hbar_f \mathbf{N}_f\left[\hat{f}(\eta,p)\right], \tag{21}$$

$$(1-p)\mathbf{L}_\theta[\hat{\theta}(\eta,p)-\theta_0(\eta)] = p\hbar_\theta \mathbf{N}_\theta\left[\hat{\theta}(\eta,p),\hat{f}(\eta,p)\right], \tag{22}$$

$$\hat{f}(0;p)=\alpha\frac{1-n}{1+n},\quad \hat{f}'(0;p)=1,\quad \hat{f}'(\infty;p)\to 0,\quad \hat{\theta}(0;p)=0,\quad \hat{\theta}(\infty;p)\to 0, \tag{23}$$

$$\mathbf{N}_f\left[\hat{f}(\eta;p)\right] = \frac{\partial^3\hat{f}(\eta,p)}{\partial\eta^3} + \beta\left(\begin{array}{l}(3n-1)\ \hat{f}(\eta;p)\dfrac{\partial\hat{f}(\eta;p)}{\partial\eta}\dfrac{\partial^2\hat{f}(\eta;p)}{\partial\eta^2} - \dfrac{2n(n-1)}{n+1}\left(\dfrac{\partial\hat{f}(\eta;p)}{\partial\eta}\right)^3\\ +\eta\dfrac{n-1}{2}\left(\dfrac{\partial\hat{f}(\eta;p)}{\partial\eta}\right)^2\dfrac{\partial^2\hat{f}(\eta;p)}{\partial\eta^2} - \dfrac{n+1}{2}\hat{f}^2(\eta;p)\dfrac{\partial^3\hat{f}(\eta;p)}{\partial\eta^3}\end{array}\right)$$
$$-\frac{2n}{n+1}\left(\frac{\partial\hat{f}(\eta,p)}{\partial\eta}\right)^2 + \hat{f}(\eta,p)\frac{\partial^2\hat{f}(\eta,p)}{\partial\eta^2}, \tag{24}$$

$$\mathbf{N}_\theta\left[\hat{\theta}(\eta;p),\hat{f}(\eta;p)\right] = \left(1+\varepsilon\hat{\theta}(\eta;p)\right)\frac{\partial^2\hat{\theta}(\eta;p)}{\partial\eta^2} + \varepsilon\left(\frac{\partial\hat{\theta}(\eta;p)}{\partial\eta}\right)^2$$
$$+\Pr\hat{f}(\eta,p)\frac{\partial\hat{\theta}(\eta;p)}{\partial\eta} + \Pr\gamma\left(\begin{array}{l}\dfrac{n-3}{2}\hat{f}(\eta;p)\dfrac{\partial\hat{f}(\eta;p)}{\partial\eta}\dfrac{\partial\hat{\theta}(\eta;p)}{\partial\eta}\\ -\dfrac{n+1}{2}\left(\dfrac{\partial\hat{f}(\eta;p)}{\partial\eta}\right)^2\dfrac{\partial^2\hat{\theta}(\eta;p)}{\partial\eta^2}\end{array}\right), \tag{25}$$

Where $p \in [0,1]$ is embedding parameter and $\hbar_f$ and $\hbar_\theta$ are the non-zero auxiliary parameters.

MTH-ORDER DEFORMATION PROBLEMS

$$\mathbf{L}_f\left[f_m(\eta)-\chi_m f_{m-1}(\eta)\right] = \hbar_f\mathbf{R}_m^f(\eta), \tag{26}$$

$$\mathbf{L}_\theta\left[\theta_m(\eta)-\chi_m\theta_{m-1}(\eta)\right] = \hbar_\theta\mathbf{R}_m^\theta(\eta), \tag{27}$$

$$f_m(0)=0,\ f_m'(0)=0,\ f_m'(\infty)=0,\ \theta_m(0)=0,\ \theta_m(\infty)=0, \tag{28}$$

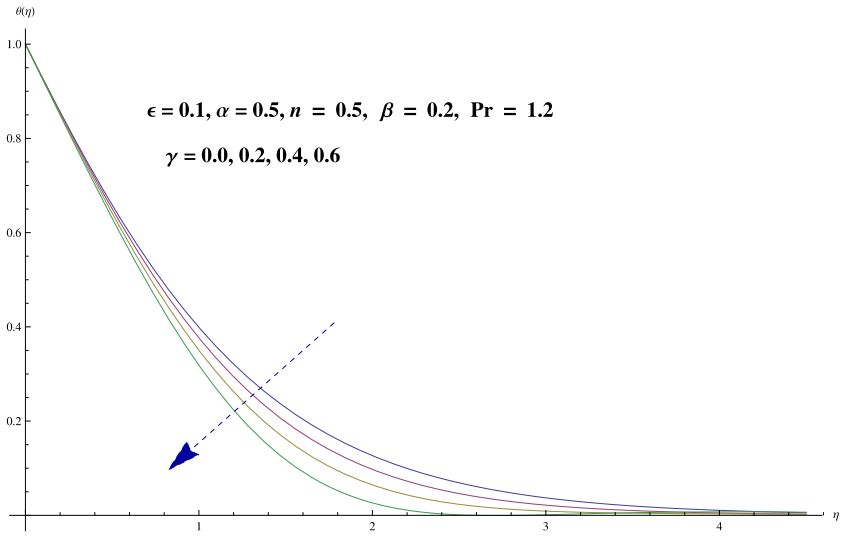

FIG. 9. Effect of γ on θ.

$$\mathbf{R}_m^f(\eta) = f'''_{m-1} + \sum_{k=0}^{m-1}\left(f_{m-1-k}f''_k - \frac{2n}{1+n}f'_{m-1-k}f'_k\right) + \beta\left(\sum_{k=0}^{m-1} f_{m-1-k}\sum_{l=0}^{k}\begin{pmatrix}(3n-1)\ f'_{k-l}f''_l \\ -\dfrac{n+1}{2}f_{k-l}f'''_l\end{pmatrix}\right)$$
$$+\beta\left(\sum_{k=0}^{m-1} f'_{m-1-k}\sum_{l=0}^{k}\left(\eta\frac{(n-1)}{2}f'_{k-l}f''_l - \frac{2n(n-1)}{n+1}f'_{k-l}f'_l\right)\right), \tag{29}$$

$$\mathbf{R}_m^\theta(\eta) = \theta''_{m-1} + \varepsilon\sum_{k=0}^{m-1}\theta_{m-1-k}\theta''_k + \varepsilon\sum_{k=0}^{m-1}\theta'_{m-1-k}\theta'_k + \Pr\sum_{k=0}^{m-1} f_{m-1-k}\theta'_k$$
$$+\Pr\gamma\left(\sum_{k=0}^{m-1} f_{m-1-k}\sum_{l=0}^{k}\left(\frac{n-3}{2}f'_{k-l}\theta'_l - \frac{n+1}{2}f_{k-l}\theta''_l\right)\right), \tag{30}$$

$$\chi_m = \begin{cases}0, & m \le 1\\ 1, & m > 1\end{cases}. \tag{31}$$

For $p = 0$ and $p = 1$, we can write

$$\hat{f}(\eta;\,0) = f_0(\eta), \quad \hat{f}(\eta;\,1) = f(\eta), \tag{32}$$
$$\hat{\theta}(\eta;\,0) = \theta_0(\eta), \quad \hat{\theta}(\eta;\,1) = \theta(\eta), \tag{33}$$

and with the variation of p from 0 to 1, $f(\eta;\,p)$ and $\widehat{\theta}(\eta;\,p)$ vary from the initial solutions $f_0(\eta)$ and $\theta_0(\eta)$ to the final solutions $f(\eta)$ and $\theta(\eta)$ respectively. By Taylor's series we have

$$f(\eta;\,p) = f_0(\eta) + \sum_{m=1}^{\infty} f_m(\eta)\,p^m, \quad f_m(\eta) = \left.\frac{1}{m!}\frac{\partial^m f(\eta;\,p)}{\partial p^m}\right|_{p=0}, \tag{34}$$

$$\widehat{\theta}(\eta;\,p) = \theta_0(\eta) + \sum_{m=1}^{\infty}\theta_m(\eta)\,p^m, \quad \theta_m(\eta) = \left.\frac{1}{m!}\frac{\partial^m \widehat{\theta}(\eta;\,p)}{\partial p^m}\right|_{p=0}, \tag{35}$$

The value of auxiliary parameter is chosen in such a way that the series (34) to (35) converge at $p = 1$ i.e.

$$f(\eta) = f_0(\eta) + \sum_{m=1}^{\infty} f_m(\eta), \tag{36}$$

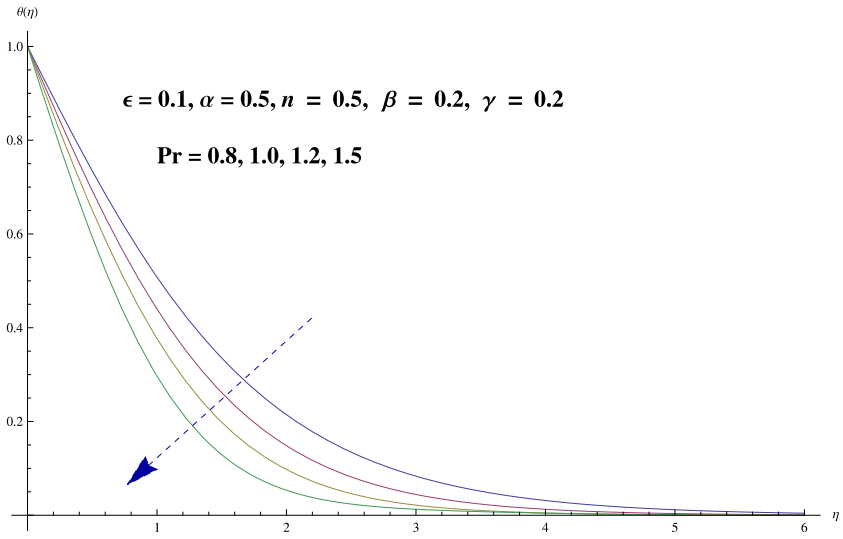

FIG. 10. Effect of Pr on θ.

$$\theta(\eta) = \theta_0(\eta) + \sum_{m=1}^{\infty} \theta_m(\eta), \tag{37}$$

The general solutions (f_m, θ_m) of Eqs. (26) and (27) in terms of special solutions (f_m^*, θ_m^*) are given by

$$f_m(\eta) = f_m^*(\eta) + A_1 + A_2 e^{\eta} + A_3 e^{-\eta}, \tag{38}$$

$$\theta_m(\eta) = \theta_m^*(\eta) + A_4 e^{\eta} + A_5 e^{-\eta}, \tag{39}$$

where the constants A_i ($i = 1, 2, \ldots, 5$) through the boundary conditions (28) have the values

$$A_2 = A_4 = 0, \quad A_3 = \left.\frac{\partial f_m^*(\eta)}{\partial \eta}\right|_{\eta=0}, \quad A_1 = -A_3 - f_m^*(0), \quad A_5 = -\theta_m^*(0). \tag{40}$$

CONVERGENCE ANALYSIS

To develop the series solutions by homotopy analysis technique it is also essential to check their convergence. Convergence region is the region parallel to $\hbar$-axis. Therefore we have plotted the $\hbar$-curves in the Fig. 2. It is found that the admissible ranges of the auxiliary parameters $\hbar_f$ and $\hbar_\theta$ are $-1.5 \leq \hbar_f \leq -0.5$ and $-1.3 \leq \hbar_\theta \leq -0.3$.

DISCUSSION

Description of various pertinent parameters on the velocity and temperature distributions is the main objective of this section. Impact of Deborah number (in terms of relaxation time) β on velocity distribution is illustrated in Fig. 3. It is noted that velocity distribution shows decreasing behavior corresponding to higher values of Deborah number. In fact Deborah number is the ratio of relaxation to observation times. So with increase in Deborah number relaxation time also increases which provides more resistance to the fluid motion. Therefore velocity profile decreases. Behavior of wall thickness parameter α on the velocity profile is sketched in Fig. 4. Higher values of wall thickness parameter result in the reduction of velocity profile and momentum boundary layer thickness for $n < 1$. As we increase the wall thickness parameter for $n < 1$, stretching velocity decreases which results in reduction of velocity profile. Analysis of power index non velocity distribution is sketched in Fig. 5. It is noted that velocity distribution shows increasing behavior corresponding to higher

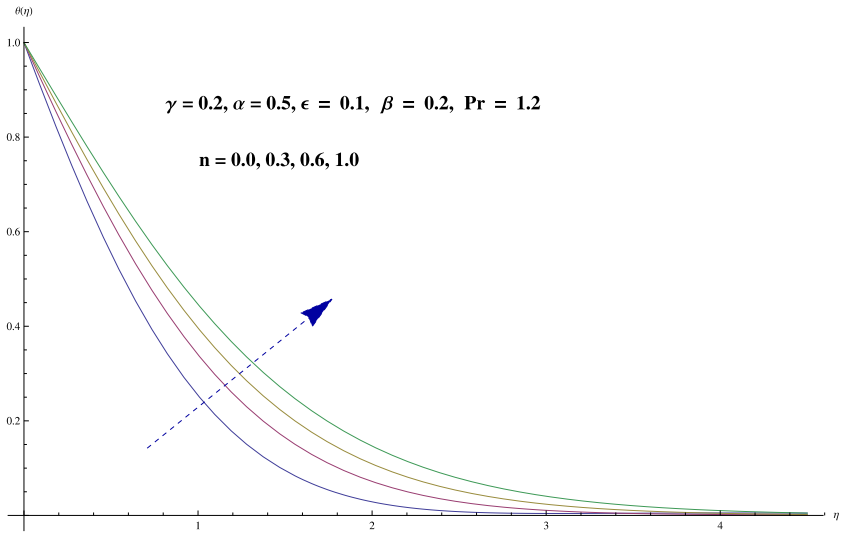

FIG. 11. Effect of n on θ.

TABLE I. Convergence of series solutions for different order of approximations when $\gamma = 0.2, n = 1.5, \beta = 0.2, \varepsilon = 0.1, \Pr = 1.2$ and $\alpha = 0.5$.

Order of approximations	$-f''(0)$	$\theta'(0)$
1	1.0493	0.7904
5	1.0849	0.5691
9	1.0861	0.5454
15	1.0861	0.5422
20	1.0861	0.5422
25	1.0861	0.5422

values of n. In fact stretching velocity increases as we increase the values of n which produces more deformation in the fluid. Hence velocity distribution increases. Characteristics of Deborah number β on temperature distribution is displayed in Fig. 6. Temperature distribution increases for larger values of Deborah number. Because higher Deborah number corresponds to larger relaxation time which provides resistance to the fluid motion and as a result more heat is produced. Therefore temperature distribution increases. Behavior of wall thickness parameter α on temperature profile is shown in Fig. 7. It is concluded that temperature distribution as well as thermal boundary layer thickness decrease for higher wall thickness parameter. It is due the fact that as we increase the wall thickness parameter less heat is transferred from sheet to the fluid. Hence temperature profile decreases. Fig. 8 discloses the behavior of thermal conductivity parameter ε on temperature profile. Higher values of thermal conductivity parameter result in enhancement of temperature profile. Physically, as we increase the thermal conductivity parameter, thermal conductivity of the fluid increases. So more heat is transferred from sheet to the fluid and consequently temperature profile increases. Impact of thermal relaxation parameter γ on temperature distribution is illustrated in Fig. 9. Temperature distribution is a decreasing function of thermal relaxation parameter. Further it is also analyzed that thermal boundary layer thickness decreases. It is due to fact that as we increase the thermal relaxation parameter, particles of the material require more time to transfer heat to its neighboring particles. In other words we can say that for higher values of thermal relaxation parameter material shows a non-conducting behavior which is responsible in reduction of temperature distribution. Further it is also noted that for $\gamma = 0$ heat transfers promptly throughout the material. Therefore temperature distribution is higher for $\gamma = 0$ i.e., for Fourier's law as compared to Cattaneo-Christov heat flux model. Analysis of Prandtl number Pr on temperature profile is displayed in Fig. 10. Higher values of Prandtl number result in the reduction of temperature profile

as well as thermal boundary layer thickness. Prandtl number is the ratio of momentum to thermal diffusivities. So higher prandtl number corresponds to lower thermal diffusivity which is responsible in reduction of temperature profile. Influence of power index n on temperature distribution is shown in Fig. 11. Temperature distribution increases for higher values of n. Further it is also noted that thermal boundary layer thickness increases.

Table I shows the convergence of the series solutions for different order of approximations. It is noted that 9^{th} and 15^{th} order of approximations are sufficient for the convergence of momentum and energy equations respectively.

CLOSING REMARKS

We have investigated the characteristics of forced convection boundary layer flow of Maxwell fluid induced by stretching sheet with variable thickness. Cattaneo-Christov heat flux model is imposed to disclose the heat transfer characteristics of variable thermal conductivity vis- coelastic fluid. The main observations are summarized as follows:

- Higher values of Deborah number result in the reduction of velocity and momentum boundary layer thickness.
- Velocity distribution shows decreasing behavior for larger values of wall thickness parameter when $n < 1$.
- Temperature distribution is higher in the case of Fourier's law as compared to Cattaneo-Christov heat flux model.
- Variable conductivity parameter results in enhancement of temperature distribution.
- Velocity and temperature distributions enhance for larger values of n.

ACKNOWLEDGMENT

This project was funded by the Deanship of Scientific Research (DSR), King Abdulaziz University, Jeddah, Saudi Arabia under grant no. (31-130-36-HiCi). The authors, therefore, acknowledge with thanks DSR technical and financial support.

[1] J. B. J. Fourier, Theorie analytique De La chaleur, Paris, 1822.
[2] C. Cattaneo, "Sulla conduzione del calore," Atti Semin. Mat. Fis. Univ. Modena Reggio Emilia **3**, 83–101 (1948).
[3] C. I. Christov, "On frame indifferent formulation of the Maxwell-Cattaneo model of finite speed heat conduction," Mech. Res. Commun. **36**, 481–486 (2009).
[4] B. Straughan, "Thermal convection with the Cattaneo-Christov model," Int. J. Heat Mass Transfer **53**, 95–98 (2010).
[5] V. Tibullo and V. Zampoli, "A uniqueness result for the Cattaneo-Christov heat conduction model applied to incompressible fluids," Mech. Res. Commun. **38**, 77–99 (2011).
[6] S. Han, L. Zheng, C. Li, and X. Zhang, "Coupled flow and heat transfer in viscoelastic fluid with Cattaneo-Christov heat flux model," Appl. Math. Lett. **38**, 87–93 (2014).
[7] M. Mustafa, "Cattaneo-Christov heat flux model for rotating flow and heat transfer of upper convected Maxwell fluid," AIP Advances **5**, 047109 (2015).
[8] L. Zheng, L. Wang, and X. Zhang, "Analytic solutions of unsteady boundary flow and heat transfer on a permeable stretching sheet with non-uniform heat source/sink," Commun. Nonlinear Sci. Numer. Simulat. **16**, 731–740 (2011).
[9] M. M. Rashidi, N. V. Ganesh, A. K. A. Hakeem, and B. Ganga, "Buoyancy effect on MHD flow of nanofluid over a stretching sheet in the presence of thermal radiation," J. Mol. Liqu. **198**, 234–238 (2014).
[10] X. Su, L. Zheng, X. Zhang, and J. Zhang, "MHD mixed convective heat transfer over a permeable stretching wedge with thermal radiation and Ohmic heating," Chem. Eng. Sci. **78**, 1–8 (2012).
[11] M. Turkyilmazoglu, "Three dimensional MHD flow and heat transfer over a stertching/shrinking surface in a viscoelastic fluid with various physical effects," Int. J. Heat Mass Transfer **78**, 150–155 (2014).
[12] L. Zheng, J. Niu, X. Zhang, and Y. Gao, "MHD flow and heat transfer over a porous shrinking surface with velocity slip and temperature jump," Math. Comptuer Model. **56**, 133–144 (2012).
[13] T. Hayat, S. Asad, M. Mustafa, and A. Alsaedi, "MHD stagnation point flow of Jeffrey fluid over a convectively heated stretching sheet," Computers & Fluids **108**, 179–185 (2015).
[14] L. Zheng, N. Liu, and X. Zhang, "Maxwell fluids unsteady mixed flow and radiation heat transfer over a stretching permeable plate with boundary slip and nonuniform heat Source/Sink," ASME J. Heat Transfer **135**, 031705 (2013).
[15] S. Mukhopadhyay, K. Bhattacharyya, and G. C. Layek, "Mass transfer over an exponentially stretching porous sheet embedded in a stratified medium," Chem. Eng. Commun. **201**, 272–286 (2014).
[16] T. Hayat, Z. Hussain, M. Farooq, A. Alsaedi, and M. Obaid, "Thermally stratified stagnation point flow of an Oldroyd-B fluid," Int. J. Nonlinear Sci. Numer. Simul. **15**, 77–86 (2014).

[17] M. Sheikholeslami and D. D. Ganji, "Numerical investigation for two phase modeling of nanofluid in a rotating system with permeable sheet," J. Mol. Liq. **194**, 13–19 (2014).
[18] T. Fang, J. Zhang, and Y. Zhong, "Boundary layer flow over a stretching sheet with variable thickness," Appl. Math. Comput. **218**, 7241–7252 (2012).
[19] M. M. Khader and A. M. Megahed, "Numerical solution for boundary layer flow due to a nonlinearly stretching sheet with variable thickness and slip velocity," Eur. Phys. J. Plus **128**, 100 (2013).
[20] M. S. A. Wahed, E. M. A. Elbashbeshy, and T. G. Emam, "Flow and heat transfer over a moving surface with non-linear velocity and variable thickness in a nanofluids in the presence of Brownian motion," Appl. Math. Comput. **254**, 49–62 (2015).
[21] S. J. Liao, *Homotopy analysis method in non-linear differential equations* (Springer and Higher Education Press, Heidelberg, 2012).
[22] S. Abbasbandy, M. S. Hashemi, and I. Hashim, "On convergence of homotopy analysis method and its application to fractional integro-differential equations," Quaestiones Mathematicae **36**, 93–105 (2013).
[23] T. Hayat, M. Farooq, and A. Alsaedi, "Thermally stratified stagnation point flow of Casson fluid with slip conditions," Int. J. Numer. Methods Heat Fluid Flow **25**, 724–748 (2015).
[24] M. Turkyilmazoglu, "Solution of the Thomas-Fermi equation with a convergent approach," Commun. Nonlinear Sci. Numer. Simulat. **17**, 4097–4103 (2012).
[25] S. A. Shehzad, T. Hayat, M. S. Alhuthali, and S. Asghar, "MHD three-dimensional flow of Jeffrey fluid with Newtonian heating," J. Central South Univ. **21**, 1428–1433 (2014).
[26] M. M. Rashidi, N. Kavyani, and S. Abelman, "Investigation of entropy generation in MHD and slip flow over a rotating porous disk with variable properties," Int. J. Heat Mass Transfer **70**, 892–917 (2014).